Force Generation and Dynamics of Individual Cilia under External Loading

David B. Hill,[†††] Vinay Swaminathan,[‡††] Ashley Estes,[§††] Jeremy Cribb,[¶††] E. Timothy O'Brien,[§††] C. William Davis,[‖††] and R. Superfine[§††*]

[†]Cystic Fibrosis/Pulmonary Research and Treatment Center, [‡]Curriculum in Applied Sciences and Engineering, [§]Department of Physics and Astronomy, [¶]Department of Biomedical Engineering, [‖]Department of Cell and Molecular Physiology, and [††]Virtual Lung Project, University of North Carolina at Chapel Hill, Chapel Hill, North Carolina

ABSTRACT Motile cilia are unique multimotor systems that display coordination and periodicity while imparting forces to biological fluids. They play important roles in normal physiology, and ciliopathies are implicated in a growing number of human diseases. In this work we measure the response of individual human airway cilia to calibrated forces transmitted via spot-labeled magnetic microbeads. Cilia respond to applied forces by 1), a reduction in beat amplitude (up to an 85% reduction by 160–170 pN of force); 2), a decreased tip velocity proportionate to applied force; and 3), no significant change in beat frequency. Tip velocity reduction occurred in each beat direction, independently of the direction of applied force, indicating that the cilium is "driven" in both directions at all times. By applying a quasistatic force model, we deduce that axoneme stiffness is dominated by the rigidity of the microtubules, and that cilia can exert 62 ± 18 pN of force at the tip via the generation of 5.6 ± 1.6 pN/dynein head.

INTRODUCTION

Cilia were one the first organelles to be studied under a microscope and are ubiquitous throughout living systems, from single-cell organisms to humans (1,2). In human physiology, motile cilia play important roles in embryogenesis, transport of cerebrospinal fluid, reproductive processes, and mucociliary clearance, among other functions (3,4). Defects in ciliary function are associated with a growing number of diseases, such as situs inversus, Bardet-Biedl syndrome, and polycystic kidney disease (5–8). Within the lung, the coordinated metachronal wave patterns of cilia, oscillating at 10–20 Hz, propel the mucus layer toward the throat (9,10). In diseases such as cystic fibrosis and chronic obstructive pulmonary disease, the protective mucus layer thickens and mucociliary clearance breaks down, leading to inflammation along the airways and an increased rate of infection (11–13). Models of ciliary propulsion of fluids depend upon an understanding of the forces generated by cilia, and the internal mechanisms that determine beat shape, amplitude, and frequency. What force can a cilium generate? Is a decrease in ciliary beat frequency (CBF) a necessary consequence of loading? At what viscosity should mucus propulsion to begin to fail? Answers to these questions will help elucidate the transition from healthy epithelial function to pathology, and the role of potential regulatory mechanisms in epithelial function.

To date, only a limited number of studies have examined the force produced by cilia or flagella against an external load. Calibrated microneedles have been used to study the force production of the compound abfrontal gill ''cilium'' (50 mm long) of the mollusk *Mytilus edulis* (14,15), as well as the arresting behavior of a bull sperm flagellum (also ~50 mm long) (16). Most recently, an atomic force microscope was used to measure the force generated from a patch of cultured esophageal cilia from the frog *Rana ribiunda*, and to estimate the force produced by an individual cilium (17). In the study presented here, we directly measured the force response of individual cilia from the human airway using spot-labeled 2.8 μm diameter magnetic microbeads and a custom-designed magnetic tweezers apparatus (a three-dimensional force microscope (3DFM) (18–20)). Tracking the labeled tips with high spatial and temporal resolution allowed us to assess the effects of applied force on the frequency, amplitude, projected beat shape, and instantaneous velocity of the cilia beat cycle. Our measurements show that cilia generate similar forces in both the effective and recovery strokes, and that the beat frequency remains constant even when the applied forces cause the beat amplitude to decrease by 85%. We conclude that beat frequency is determined by an internal timing mechanism and not by geometrical switch points. By applying a simple model, we were able to determine that the spring constant of the axoneme during actuation is dominated by the microtubules (MTs), that the effective force generated by the coordinated action of the molecular motors is ~62 pN, and that a cilium will react by decreased amplitude to any appreciable increase in load.

MATERIALS AND METHODS

Normal human bronchial epithelial cells were cultured on a 0.4 μm pore-sized Millicell (Millipore, Billerica, MA) coated with collagen and maintained in air-liquid interface media (UNC Tissue Core) as previously described (21). Over a period of 6 weeks, confluent cultures develop cilia and are able to transport mucus. Once the cultures were well ciliated, they were washed twice for 20 min in phosphate-buffered saline (PBS, Invitrogen (GIBCO), Carlsbad, CA) to remove the bulk of the mucus layer. They were then incubated at 37°C for 30 min in 50 μM ATP (Sigma Aldrich, St. Louis,

Submitted April 29, 2009, and accepted for publication September 15, 2009.

*Correspondence: rsuper@physics.unc.edu

Editor: Denis Wirtz.

0006-3495/10/01/0057/10 $2.00

doi: 10.1016/j.bpj.2009.09.048

MO) in PBS to stimulate the cells to release all stored mucins (22). After mucin secretion was stimulated, the cultures were washed twice for 10 min in PBS and then washed for 10 min in 10 mM dithiothreitol (DTT) (Sigma Aldrich, St. Louis, MO) in PBS. After two additional PBS washes to remove all free DTT and remaining mucus, the cultures were incubated in biotinylated wheat-germ agglutinin (b-WGA; Vector Laboratories, Burlingame, CA) for 15 min. The cultures were washed twice for 10 min in PBS after b-WGA incubation, and then incubated at 4°C for 30 min in <1% v/v spot-labeled (see the Supporting Material) streptavidin-coated 2.8 μm magnetic beads (DYNAL Biotech, Oslo, Norway). The cultures were then washed one final time, and the cell layer(s) and underlying membrane were then removed from the culture dish and transferred onto a number 0 coverslip to be loaded into the 3DFM for force-response experiments.

The UNC 3DFM was used to apply forces to the magnetic beads attached to cilia (18–20). The instrument combines a conventional optical microscope with super paramagnetic beads as mechanical probes. The forces are generated by a magnetic field gradient generated by multiple electromagnet pole tips arranged in space to provide the necessary directional capability (18–20). The cultures were viewed by transmitted light, and the motion of oscillating beads was recorded at 120 fps by means of a high-speed video camera (Pulnix; JAI, CA). Bead position was determined using Video Spot Tracker (Center for Computer Integrated Systems for Microscopy and Manipulation; http://cismm.cs.unc.edu/downloads/).

RESULTS

Baseline ciliary beat pattern

We attached a spot-labeled 2.8 μm diameter magnetic bead to the cilia tip, both to transmit force to individual cilia and to track the two-dimensional projection of the cilia's motion with high spatial and temporal resolution (Fig. 1). Commercial streptavidin-labeled superparamagnetic beads (Dynabead, Invitrogen) were coated with gold, except for a small (~100 nm diameter) area to ensure that each bead could bind to only one cilium (see the Supporting Material). Before the application of magnetic force by the 3DFM, the average ciliary beat amplitude (CBA) for cilia attached to a bead was 5.5 μm ± 0.3 μm (n = 15), which is in good agreement with published results (5). The average CBF of the cilia in our experiment was 8.5 Hz ± 0.3 Hz, also in agreement with published results obtained at 23°C (23).

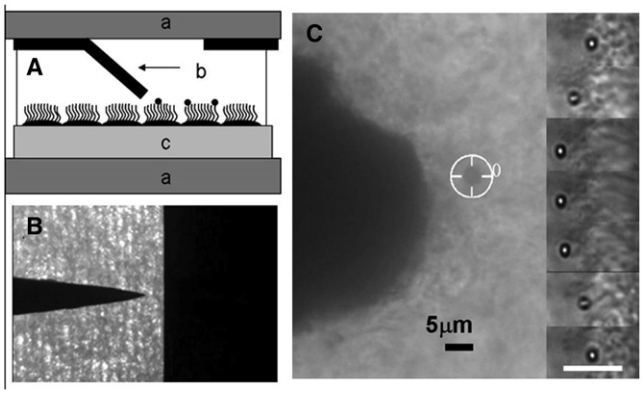

FIGURE 1 (*A*) Schematic of the 3DFM in pole-flat configuration: (*a*) a pair of coverglasses separated by ~200 μm; (*b*) one pole tip bent toward the substrate, the "flat" fixed on upper glass labeled *a*; and (*c*) cells grown on Millicell membrane. (*B*) Top-view image of the pole-flat, thin-film magnetics. (*C*) Bright-field image (40×, 0.6 NA objective, and 1.5 image magnifier) of a 2.8 μm magnetic bead (tracking cursor in place) attached to beating cilia in the 3DFM. The pole tip is clearly visible 12 μm away. The inserted images on the right-hand side are time-series images (0.083 ms apart) of a 1 μm bead bound to beating cilia. A 5 μm scale bar is shown.

As expected from earlier work (24), an asymmetry was observed in the beat pattern (see Fig. 2, *A–D*). Based on extrapolations from the beat shape of rabbit tracheal cilia as a function of time (24), and human airway cilia (25) (see the Supporting Material), we believe the effective stroke to be the stroke in which a cilium reaches the highest velocity and begins to slow gradually ~2/3 of the way through that stroke (*dark arrows*, Fig. 2 *C*). In contrast, the velocity during the recovery stroke was more constant, with a more rapid transition between the recovery and effective strokes (*lighter arrows*).

The average maximum velocity reached during the effective stroke, $\overline{V}_E$, was 198 μm/s ± 15 μm/s, and during the recovery stroke the average maximum velocity, $\overline{V}_R$, was 155 μm/s ± 11μm /s (n = 15). We found that the baseline motion of cilia-bound beads was largely planar, with the lateral excursion of the cilium tip being 5% of the principal beat amplitude, consistent with previous measurements (26). We also note that the drag force calculated for a 2.8 μm bead at the maximum velocity reached during the power stroke of the cilia's beat (~200 μm/s) moving through buffer is ~5 pN. As presented below, this is <1/10th the effective cilia force determined by our measurements. Taken together, these results argue that bead attachment does not significantly alter the characteristic cilium beat pattern.

Cilia force response

Forces in our system were applied either toward or against the effective stroke. Parsing the data derived from forces applied toward or against the effective stroke allowed us to determine that the effect of load is independent of orientation. To illustrate the effect of forces toward and away from the effective stroke, we show representative data in Fig. 2 for cases in which the load was toward (*i*) or away from (*ii*) the effective stroke, although in this example a different magnitude of force pulses was applied to each (142 pN in *i*, 59 pN in *ii*). The duration of the applied maximum force was limited by the detachment of the bead from the cilium at longer times and high forces. No matter which way the forces were applied, the cilia reacted in the same characteristic manner: the center of oscillation moved toward the applied force (Fig. 2 *A*; force oriented toward the top of the page for both *i* and *ii*), CBA decreased markedly, and CBF was unaffected. The response to the force applied in Fig. 2 *A* is shown in Fig. 2 *B*, and a close-up of the beat pattern in time, before and during a pull, is shown in Fig. 2 *C*. Note that the period of oscillation was unchanged while the amplitude decreased significantly. Given the constant frequency observed through the experiments, the tip velocity of the cilia must decrease proportionally to

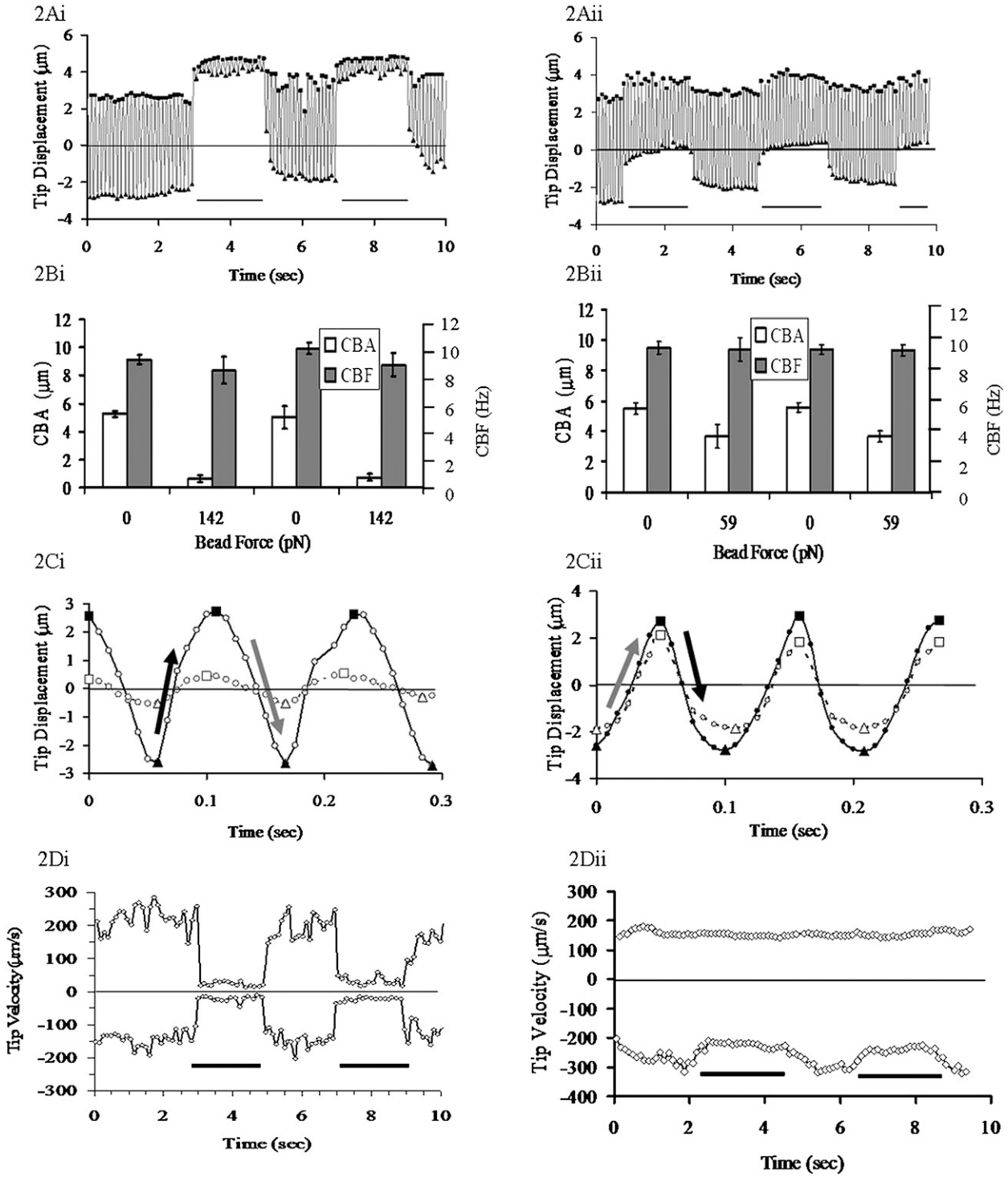

FIGURE 2 Cilia beat pattern in the pulse experiments: (*i*) effective stroke in the direction of the bead (magnetic) force, and (*ii*) recovery stroke in the direction of the bead force. (*A*) Position versus time trace of 2.8 μm beads attached to a human bronchial epithelial cilium. The line at the base of the graph indicates force on/off. (*B*) CBA and CBF with and without the applied bead force. (*C*) Closer inspection of the cilia beat pattern with the force on (*solid line*) and off (*dashed line*) from panel *A*. The line is the bead's motion, the squares are the local maximums, and the triangles are the local minimums. The gray arrows indicate the effective stroke of the cilia, and the black arrows the recovery stroke. (*D*) Instantaneous maximum velocity of beating cilia for the tip position data in panel *A*. In all charts, the position/velocity scale is oriented to be in the direction of the external force.

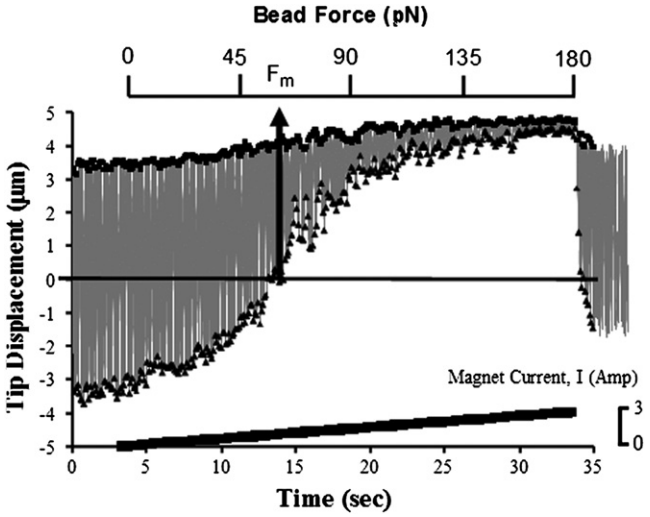

FIGURE 3 Reduction of the CBA in force-ramp experiments. The gray line indicates the path of the bead, with squares indicating the local maximum and triangles the local minimum. The line at the bottom of the figure shows the magnetic driving current; the bead force is shown on a separate horizontal axis. Using our model, the point at which the bead force is sufficient to limit the minimum excursion of the bead to be the midpoint of the baseline motion is defined as the motor force. The position scale is oriented to be in the direction of the external force.

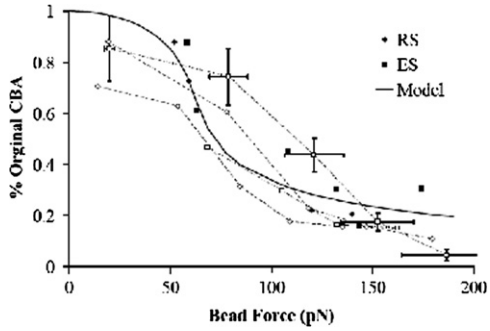

FIGURE 4 Effect of external force (F_B) on the CBA. Cilia beating with their effective stroke in the direction of the bead force are represented by squares ($n = 9$), and cilia beating with their recovery stroke in the direction of the bead force are shown with diamonds ($n = 6$). Solid data points are from pulse-type experiments, and open points are from force-ramp experiments. Data from the same ramp are connected with a dotted line.

the decrease in beat amplitude, as shown in Fig. 2 *D*. It is noteworthy that the velocity of both the effective and recovery strokes is decreased in response to the application of the external force, and that the ratio of the velocities stays relatively constant, regardless of the orientation of the beat pattern to the external force. If this were not true, one would expect the beat pattern shown in Fig. 2 *C* to show a sawtooth wave when the cilium is loaded, altering the ratio between $\overline{V}_R$ and $\overline{V}_E$ depending on the cilium's beat orientation with respect to the external force, which is not the case.

Forces were also applied as a slow ramp (Fig. 3), such that coil currents to the magnets were raised as a linear function over 30 s to produce ~170 pN force at the bead and then removed. This much longer application of force also did not alter the CBF, whereas the CBA gradually decreased to <10% of the starting value. By analyzing these ramp-type experiments within the context of the model we present below, we were able to deduce the effective motor force exerted by the motor proteins within the cilium.

Cilia do not stall

A comparison of our methodology with that applied to single-molecule motors (27) might imply that at some characteristic force the cilium would stop oscillating altogether. However, we found that although CBA declined with increasing force, forces approaching 200 pN did not stall the beat (Figs. 3 and 4). Higher forces tended to pull the beads off of the cilium, but did not appear to stall the oscillation, even briefly. For convenience, we define an ''effective stall force'' as the point at which the CBA has been reduced to 15% of its baseline. Combining all force/CBA data, we looked for forces whose error bars overlapped the 15% reduction line. These forces centered on 163 pN ± 18 pN ($n = 15$).

Although our experiment was fundamentally different from previous cilia and flagella force measurements, it is noteworthy that our results are of the same order of magnitude as previous studies on bull sperm flagella. Those studies showed an induced arrest behavior at 250 pN (16), but did not report the detailed amplitude change as the load was increased. A recent atomic force microscopy measurement of the ensemble average of the normal (i.e., perpendicular to the epithelial) force generated by frog esophageal cilia during their effective stroke was interpreted to be equivalent to 210 pN per cilia (17).

Model

It is tempting to conclude that the motors within a cilium together exert a force ''at least'' as large as this 162 pN, and that, for example, this force can be applied to propel fluids. However, in our experiment, the external force is applied to the entire mechanical structure of the axoneme and not directly to the internal motor proteins. The external applied force and the internal motors act in parallel against the mechanical stiffness of the axoneme to produce a bend shape, and hence a tip displacement, which one must take into account when interpreting the true force produced within a cilium. We present a simple mechanical model that allows us to separately quantify the axonemal stiffness and the effective internal force generated by the collective action of the axonemal motors (available for motility or fluid propulsion). The model also allows us to predict the magnitude of the fluid resistive force at which cilium motion would begin to be compromised.

Because ciliary motion appears to be determined by a force balance at all points in its cycle, and inertia can be neglected at this length scale, the cilium can be described as being in quasistatic equilibrium. In such a model, the forces derived

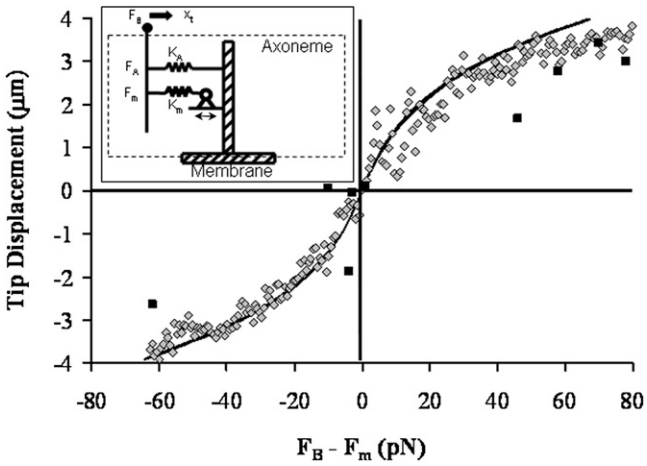

FIGURE 5 Axoneme spring constant fit to data. Data points (*diamonds*) are the local minimums from Fig. 3, and the black squares are the pulse data ($n = 9$). The data have been replotted such that the applied force (i.e., the sum of the external force F_B, and the effective motor force, F_M) fall at 0,0. The line is from the nonlinear model with parameters determined by fit to the complete cilia data set of Fig. 4, which is in good agreement with the data. Inset: Schematic of a one-dimensional model for the axoneme with force F_B applied to the bead attached to the tip. The axoneme is represented as a nonlinear spring K_A that applies a restoring force F_A, and an internal force F_m generated by an internal spring K_m extended by a system of stepping motors.

from internal motors (F_m), from the mechanical characteristics of the axoneme (F_A), and from the forces applied by the magnetic bead (F_B) sum to zero at all times ($F_B + F_m + F_A = 0$). For simplicity, we reduce the three dimensional physics of the axoneme to a single coordinate, focusing on the tip displacement along a single axis we denote as x_t. We consider the axoneme in this model to be a one-dimensional spring element with a stiffness k_A that relates the net force on the tip to its displacement through $k_A = -F_A/x_t$. The axoneme is bent by internal shear stresses that are determined by the magnitude, distribution, and direction of the forces the dynein motors generate on neighboring doublet MTs (4). The collective effect of these shear stresses within the model is to bend the axoneme as if a single force (F_m) had been applied at the tip. Finally, the bead exerts a force, F_B, to the cilium through the tip, which, once activated, is constant throughout a ciliary beat cycle. This model is diagrammed in the inset of Fig. 5. We consider F_m to be periodic, with an amplitude that is independent of the externally applied force F_B. We also neglect fluid forces at present, which for aqueous environments are calculated to be on the order of 1% of the effective motor force.

Immediately this model allows us to interpret the effective force generated by the internal motors. If we take the midpoint of the unloaded cilium beat as $x_t = 0$, then we can understand the cilia motion without load as due to the internal motor force that is at a maximum when the cilia tip is displaced the farthest from the midpoint location, at a turnaround point. Whenever the cilium tip is at $x_t = 0$, then $F_A = 0$. Without the additional load, this will also be the location where $F_m = 0$, as dictated by the force balance assumption. However, when the external load F_B is applied, the beat cycle midpoint shifts in the direction of the applied force. At a particular value of F_B, it will be the case that one of the turnaround points will be shifted to the original $x_t = 0$. At this location, $F_A = 0$ and the sum of $F_m + F_B = 0$. Therefore, at this location, we can set $F_m = -F_B$ to find the value of the effective motor force from the value of F_B that pulls one of the beat extrema to the original midpoint. It can be seen from Fig. 3 that this force for this data sequence is ~65 pN, and thus the internal forces provided by the motors within this cilium produce ~65 pN of force.

We now use this model to focus on the beat amplitude and its reduction under load. A model that assumes a linear (Hookean) spring for the axoneme, where $k_A = -F_A/x_t$ is a fixed constant independent of position, does not produce a reduction in the periodic beat amplitude as the magnetic force is increased. A model with an axoneme that stiffens at large amplitudes, with $F_A = -k_A x_t - k_A' x_t^3$, does capture the CBA reduction while also allowing the applied force to shift the center of oscillation. The particular form for F_A was chosen for simplicity. It is the lowest power exponent that provides symmetric stiffening of the axoneme (i.e., stiffening occurs similarly in both directions). We use this term to capture the qualitative features of the axoneme under load. We note that the quantitative conclusions of this report are determined from the cilium behavior near $\overline{x}_t = 0$, where the nonlinear term of the spring constant is not a significant factor. The origin of this term may be due to the mechanical stiffening of the axoneme at large bend angles arising, for example, from steric interactions in the interior of the MT structure. We will leave further analysis of this term for another report. This model was applied directly to the data. This nonlinear spring relationship correctly captures the reduction in CBA with applied force (Fig. 4). By solving our model for the beat amplitude as a function of external force (see the Supporting Material), we find $k_A = 5.4 \pm 1.43$ pN/μm, $k_A' = 0.73 \pm 0.15$ pN/μm^3, and $F_m = 62$ pN $\pm$ 18 pN, where the errors are the standard deviation of the fit. Thus the fit generates a value for F_m that is in good agreement with that obtained by inspection of Fig. 3, as described above. Moreover, when the data are plotted as a function of $F_B - F_M$ (Fig. 5), we see that this fit is in reasonably good agreement with our data in their entirety. Finally, we note that within our model, the ''stall'' force in terms of an applied force that brings the beat amplitude to zero does not exist. It is F_m that is the fundamental quantity of interest for gaining insight into axoneme dynamics and understanding the force that the cilium can apply.

DISCUSSION

Studies of a variety of model biological systems have left open the question of whether the force generation in axonemes is symmetric with regard to the stroke direction,

and whether the timing mechanism that determines the beat frequency is based on an internal timer or the external curvature of the axoneme (11,28–31). These issues play a critical role in computational models of the propulsion of fluids by cilia. For example, most models assume the so-called curvature-controlled switch-point mechanism for determining the beat frequency, which would dictate the maintenance of cilia bend shape when the cilia are loaded with a high-viscosity fluid (32). These models also require the correct value of internal force generation to predict fluid propulsion. Thus our results usefully inform several fundamental issues of cilia function. Below we develop the implications of our results with respect to the contributions of MTs on the overall stiffness of the axoneme, the effective total and per-motor force generated by the dyneins, and the control of switching between the effective and recovery strokes. We conclude with the implications of the cilia force in fluid propulsion and in rheological and flow sensing.

The stiffness of the axoneme is dominated by the contributions of the MTs

The linear spring constant we measured ($k_A = 5.4$ pN/μm) allows us to assess the relative contribution of MTs and other structural proteins within the cilium using the theory of simple bending. Assuming small deformation, $k_A = 3EI/L^3$, where E is Young's modulus of the material, I is the second moment of inertia, and L is the cilium length (7 μm (31)), we find that the flexural rigidity EI (the force required to bend a structure to a unit curvature) is $(6.2 \pm 1.6) \times 10^{-22}$ Nm^2. Two previous studies measured the stiffness of individual sperm flagellar axonemes using microneedles (16,33). Most relevant to our data is the study in which values of $3.0 - 15 \times 10^{-22}$Nm^2 were obtained in echinoderm sperm (33). Our value falls within that range. We can now compare our value with that obtained from measured mechanical properties of MTs and the established geometry of the axoneme. As a lower bound, we calculate the axoneme flexural rigidity assuming that it equals the sum of the flexural rigidities of its component MTs. This is equivalent to assuming that the MTs can slide freely past one another during bending. Directly measured values of flexural rigidity of singlet MTs fall within the range of 16×10^{-24} to 45×10^{-24} Nm^2 (34–38). We therefore calculate the ratio of flexural rigidities of an axoneme to a singlet MT, $EI_{\text{Axoneme}}/EI_{\text{SM}}$, to be given by the range of 14–19. Assuming a reasonable geometry for the axoneme, and that the flexural rigidity of the MT doublet can be extrapolated from its geometry relative to the singlet (see the Supporting Material), we calculate $EI_{\text{Axoneme}}/EI_{\text{SM}} = 28$ (38). The agreement between our measured value and calculated literature values implies that the flexural rigidity of the axoneme is dominated by the MTs, with internal proteins providing a relatively minor contribution for small bend angles during beating. We note that our measurements occur during active motion of the motors, and the linear term alone applies for small deformations. A more detailed interpretation will require direct measurements of the mechanical properties of MT doublets.

Most of the axonemal motors contribute to actuation of the axoneme

We obtained an effective internal motor force, F_m, of 62 pN $\pm$ 18 pN by fitting our model to the data in Fig. 4. To relate F_m to the contributions of individual axonemal motors, we interpret it in the context of a two-dimensional, internally driven, elastic rod-like filament model for the axoneme (39). In this model, each motor applies a force with a component parallel to the MTs, and thus generates a distributed shear stress through the action of the ensemble of motors. The shear stress acts to bend the axoneme. A uniformly distributed shear stress will bend a cantilever as if a single force were applied at the cantilever tip, F_m. We can write $F_m = n \cdot a \cdot f \cdot m$, where a is the MT doublet spacing, f is the internal shear force per motor domain, m is the density of motor domains per unit length in the axoneme, and n is the effective number of columns of active motors. Solving for f, we find $f = F_M/n \cdot a \cdot m$. The MT doublet spacing in the axoneme is known to be ~24 nm, and analyzed cryo-electron microscopy images (40) of the *Chlamydomonas* axoneme reveal the number of motor heads per repeat length of 96 nm. By counting four of the three-headed outer dynein arms, and one double-headed and five single-headed inner dynein arms, we get a total of 19 motor head domains. There is some evidence to suggest that airway cilia outer dynein arms are double-headed (41), unlike *Chlamydomonas*, yielding a total of 15 motor head domains. Based on symmetry, we can assume that there are at most four columns of dyneins that contribute to the beat in a particular direction (30), which when weighted according to their geometrical contribution (see the Supporting Material) yield $n = 2.84$. This gives us a conservative value of 5.6 pN $\pm$ 1.6 pN per motor domain in the cilia, which is in good agreement with the 6 pN stall force observed in single-molecule experiments (42). To demonstrate the sensitivity of the derived motor force on estimated parameters, we note that if the number of motor heads per repeat were the same as in *Chlamydomonas* (19), our force per motor would be 4.4 pN $\pm$ 1.3 pN.

Our results and calculations indicate that during the beat cycle, a large fraction of the dyneins are contributing to the shear stress within the axoneme. This conclusion suggests that there is little ''reserve'' force available to the axoneme. As the force due to external influences approaches ~60 pN, due, for example, to loading from viscous fluids, the axoneme should begin to significantly change its behavior.

Internal timing mechanism

Our results have significance for the switch-point hypothesis (43), and for the underlying dynamics that control the CBF. It is widely recognized that some form of strain is necessary to couple the individual motors for their coordination over

significant lengths of the axoneme (44). The cause of the switch point has been attributed to local curvature control (29,45–47) through intra-MT shear strain (45–47) at points of curvature (44,46,48,49) or an avalanche of dyneins releasing as the internal normal strain between MT pairs increases when the axoneme bends (30,50,51). We observed no change in the beat frequency upon the application of forces that decreased CBA up to 15% of the original amplitude while causing a dramatic shifting of the tip trajectory away from the center line. Although our experimental geometry prevents measurement of the axoneme's shape, we can infer that the axoneme acquires a different curvature when the tip is displaced microns away from the original center line under external loading. If the curvature of the axoneme caused a triggering of the turnaround, then we should see a reversal at approximately the same tip positions as the turnaround positions of the unloaded axoneme. Likewise, when CBA drops to 15% of its original value, we expect that the curvature of the axoneme during the beat cycle would be similarly diminished, especially for the stroke beating against the external force. However, the axoneme continues to switch beat directions with the same timing as before the application of the external force. The concept of an internal timing mechanism within the axoneme was previously suggested (28) and is supported by laser-tweezers measurements of dynein slipping, indicating a potential oscillating mechanism in force generation at the molecular scale (42,52,53). Strain coordination between motors may be due to shear strains between neighboring MTs that do not result in curvature, as may happen if the boundary condition at the basal body allows for sliding (54–56). We conclude that an internal timing mechanism dominates the switch mechanism, and that the coupling needed for coordination is robust over a wide range of external geometries.

Both effective and recovery strokes are driven

Brokaw (57) recently pointed out that models of flagellar and ciliary axoneme motion can be classified as either active effective with passive recovery, or active for both. Our data strongly support an active motion for both effective and recovery strokes in airway-derived cilia, especially given the observation that the midline of the tip velocity plot remains essentially the same during pulls as it was before, which implies that velocity is not biased in the direction of the magnetic force. This is true whether the direction of force is toward or away from the effective stroke. Thus, the tip velocity in both directions appears to be determined by the endogenous biochemistry and biophysics of the activation and release of the dynein motors during all phases of the beat.

Cilia can generate sufficient force to propel healthy mucus

The effective force that we measure for cilia has implications for the physiological roles of cilia in propelling fluids and sensing force. We can use the simple model for the force of a surrounding fluid on a moving rod to understand the ability of cilia to propel high-viscosity fluids such as mucus. The maximum torque needed to rotate a rod about its end in a viscous fluid through an angle of $\pm 45^\circ$ is given approximately by $T = (\pi^3/24)\eta L^3 f$ (27). Assuming that this torque is generated from a point force at the rod end, we find that the critical viscosity where the effective internal force can generate the necessary torque is given by $\eta_{crit} = (24/\pi^3)F_m/L^2 f$. For a 7 μm axoneme beating at 10 Hz with $F_m = 62$ pN, we find $\eta_{crit} = 100$ mPa·s. It is noteworthy that this viscosity is comparable to the measured viscosity of normal human respiratory tract mucus (58–60), is lower than the viscosities reported for mucus and sputum from patients with cystic fibrosis (61) and chronic bronchitis (62), and is ~100 times greater than the viscosity of the buffer.

The reports of viscous effects on ciliary beat phenomena include studies of CBF, beat shape, and metachronal patterns in the ciliary fields of paramecium (63), and three reports of viscosity effects in airway epithelia (64–66). All four studies reported a drop in CBF with increasing viscosity of the surrounding solution. The three studies on airway cilia showed an initial decrease in CBF at low viscosities (down to ~65% at 30 mPa·s) that remained nominally constant at higher viscosities, with the eventual loss of consistent beat shapes at viscosities above 180 mPa·s (66). The usual interpretation of these results is that the drop in CBF is an inherent mechanical effect on the cilia, whereas the maintenance of the CBF at higher viscosities is due to a regulatory mechanism correlated to Ca^+ influx, channel activity, and other biochemical effectors (3). These interpretations are consistent with curvature control models that maintain an internal force mechanism whose amplitude is unchanged under load. Such an interpretation is additionally supported by the observation of a constant amplitude under viscous loading (66). However, it is difficult to reconcile these models with our results, which show a constant CBF that is independent of beat amplitude. Our results may be consistent with previous measurements of viscous effects if we consider an induction period for the onset of the CBF decrease. Our measurements in this report are limited to <30 s due to the force-induced release of the bead, whereas all three airway cilia studies noted the reduction of the CBF over a few minutes after dosing with higher viscosity. This also may indicate a switchover between control modes, from frequency control to geometry control, as has been observed in flagellar beating (67). Alternatively, altering the viscosity of solutions to change the effective load at the cilium tip changes a large set of variables, including the ionic strength and effective mobility of nucleotides and other cofactors, which may or may not be effectively addressed. Our system allows all other variables to remain constant, except for increased loading at the tip. Finally, the forces experienced by the axoneme under viscous loading are fundamentally different from those experienced in our experiment. In viscous loading experiments, the external

drag force on the axoneme is proportional to the instantaneous axoneme velocity. In our system, the external force is constant, and therefore it is possible that these two types of experiments elicit different responses from the axoneme. Within the context of a dynamical systems model for the axoneme, altering the dissipative term through a change in viscosity can dramatically change the filament dynamics in a highly nonlinear manner (39). We hope to address this in a future report.

Cilia generate sufficient force to stimulate stretch-activated channels

Within the context of a flow system such as lung epithelia, homeostasis may be enabled by a feedback mechanism whereby cilia act as sensors of some combination of mucus flow, rheology, and volume (68). If the cilium tip end were constrained by a static, high-modulus mucus layer, then a simple model of cilia dynamics would predict that the internal drive mechanism of the axoneme would cause a force of $F_m = 62$ pN to be exerted on the membrane at the base of the axoneme. We can compare this point force to shear stresses that have provoked responses in epithelia by calculating an effective membrane shear stress σ through $\sigma = F_m c$, where c is the area density of cilia. Taking $c = 5$ cilia/μm^2 (69), we find $\sigma = 325$ Pa. This value is four orders of magnitude larger than the values of shear stress caused by fluid flow that have been shown to provoke responses in cell culture systems where values $<10^{-2}$ Pa were effective (70,71). Therefore, we would expect that a field of cilia with their tips constrained by high-viscosity mucus could cause a response through a mechanism similar to shear sensing, perhaps through strains within the membrane or underlying cytoskeleton.

CONCLUSIONS

We have presented the dynamics of individual airway epithelial cilia under load using a magnetic bead methodology. Our results imply that the mechanical stiffness of the axoneme is dominated by the MTs during activation. The shear stress that bends the axoneme, assuming measurements of in vitro assays, is generated by a large fraction of the dynein motor proteins activated at any one time. The frequency of the cilium is unchanged upon loading, even when its motion is suppressed to $<15\%$ of its original value. This challenges existing models that were designed to account for observed decreases in the CBF with increased viscosity of the surrounding fluid. These curvature-dependent models rely on geometry-dependent switch points between effective and recovery strokes. In contrast, our measurements highlight the role of an intrinsic mechanism that allows the axoneme to maintain its beat frequency under external loading. Further investigations will benefit from side-on imaging, whereby the true profile of the cilium during the application of force can be determined and compared with profiles seen in viscous loading experiments. The side profile of the beat shape can also be used to test the notion that the switch point does not require a proscribed curvature in the axoneme. Our measure of the force generated by the axoneme sets quantitative bounds on the propulsion of viscoelastic fluids, and provides a measure of the ciliary forces on the membrane that may play a role in biochemical feedback regulation of epithelial phenomena.

SUPPORTING MATERIAL

Additional text, equations, figures, and references are available at http://www.biophysj.org/biophysj/supplemental/S0006-3495(09)01560-4.

We thank John Sheehan, Sorin Mitran, Patrick Sears, Michael Falvo, and all of the members of the Virtual Lung Project for invaluable discussions, and Anderson Cox for helping with the spot-labeled bead preparations.

This work was supported by grants from the National Institutes of Health (P41-EB002025-24A1 (Computer Integrated Systems for Microscopy and Manipulation), R01-EB000761 (3DFM), and R01-HL077546-03A2 (Virtual Lung)), the National Science Foundation (CMS-0507151 (Nanoscale Interdisciplinary Research Team)), and the Cystic Fibrosis Foundation (HILL08I0).

REFERENCES

1. Dobbell, C. 1958. Antony van Leeuwenhoek and His ''Little Animals''. Russell and Russell, New York.
2. Satir, P. 1995. Landmarks in cilia research from Leeuwenhoek to us. *Cell Motil. Cytoskeleton.* 32:90–94.
3. Salathe, M. 2007. Regulation of mammalian ciliary beating. *Annu. Rev. Physiol.* 69:401–422.
4. Satir, P., and S. T. Christensen. 2007. Overview of structure and function of mammalian cilia. *Annu. Rev. Physiol.* 69:377–400.
5. Afzelius, B. A. 2004. Cilia-related diseases. *J. Pathol.* 204:470–477.
6. Eley, L., L. M. Yates, and J. A. Goodship. 2005. Cilia and disease. *Curr. Opin. Genet. Dev.* 15:308–314.
7. Marshall, W. F. 2008. The cell biological basis of ciliary disease. *J. Cell Biol.* 180:17–21.
8. Vogel, G. 2005. News focus: betting on cilia. *Science.* 310:216–218.
9. Etievant, M. 1992. Mechanisms and control of mucociliary clearance. *Bull. Inst. Pasteur.* 90:245–266.
10. Sleigh, M. A., J. R. Blake, and N. Liron. 1988. The propulsion of mucus by cilia. *Am. Rev. Respir. Dis.* 137:726–741.
11. Boucher, R. C. 2004. New concepts of the pathogenesis of cystic fibrosis lung disease. *Eur. Respir. J.* 23:146–158.
12. Hogg, J. C., F. Chu, …, P. D. Paré. 2004. The nature of small-airway obstruction in chronic obstructive pulmonary disease. *N. Engl. J. Med.* 350:2645–2653.
13. Randell, S. H., R. C. Boucher, and University of North Carolina Virtual Lung Group. 2006. Effective mucus clearance is essential for respiratory health. *Am. J. Respir. Cell Mol. Biol.* 35:20–28.
14. Yoneda, M. 1960. Force exerted by a single cilium of *Mytilus edulis*. I. *J. Exp. Biol.* 37:461–468.
15. Yoneda, M. 1962. Force exerted by a single cilium of *Mytilus edulis*. II. Free motion. *J. Exp. Biol.* 39:307–317.
16. Schmitz, K. A., D. L. Holcomb-Wygle, …, C. B. Lindemann. 2000. Measurement of the force produced by an intact bull sperm flagellum in isometric arrest and estimation of the dynein stall force. *Biophys. J.* 79:468–478.

17. Teff, Z., Z. Priel, and L. A. Gheber. 2007. Forces applied by cilia measured on explants from mucociliary tissue. *Biophys. J.* 92: 1813–1823.

18. Fisher, J. K., J. Cribb, …, R. Superfine. 2006. Thin-foil magnetic force system for high-numerical-aperture microscopy. *Rev. Sci. Instrum.* 77:023702-1–023702-9.

19. Fisher, J. K., J. R. Cummings, …, R. Superfine. 2005. Three-dimensional force microscope: a nanometric optical tracking and magnetic manipulation system for the biomedical sciences. *Rev. Sci. Instrum.* 76:053711.

20. O'Brien, E. T., J. Cribb, …, R. Superfine. 2008. Magnetic manipulation for force measurements in cell biology. *In* Biophysical Tools for Biologists, Vol. 2: In Vivo Techniques. John J. Correia and William H. Detrich III, editors. Elsevier Academic Press, San Diego, CA. 433–449.

21. Fulcher, M. L., S. Gabriel, …, S. H. Randell. 2005. Well-differentiated human airway epithelial cell cultures. *Methods Mol. Med.* 107:183–206.

22. Lethem, M. I., M. L. Dowell, …, C. W. Davis. 1993. Nucleotide regulation of goblet cells in human airway epithelial explants: normal exocytosis in cystic-fibrosis. *Am. J. Respir. Cell Mol. Biol.* 9:315–322.

23. Yager, J., T. M. Chen, and M. J. Dulfano. 1978. Measurement of frequency of ciliary beats of human respiratory epithelium. *Chest.* 73:627–633.

24. Sanderson, M. J., and M. A. Sleigh. 1981. Ciliary activity of cultured rabbit tracheal epithelium: beat pattern and metachrony. *J. Cell Sci.* 47:331–347.

25. Sears, P. R., K. Thompson, …, C. W. Davis. 2007. Empirical model of ciliary dynamics for human airway epithelium. *Proc. Biophys. Soc. Meeting, Baltimore, MD*.

26. Chilvers, M. A., and C. O'Callaghan. 2000. Analysis of ciliary beat pattern and beat frequency using digital high speed imaging: comparison with the photomultiplier and photodiode methods. *Thorax.* 55:314–317.

27. Howard, J. 2001. Mechanics of Motor Proteins and the Cytoskeleton. Sinauer Associates, Sunderland, MA.

28. Brokaw, C. J. 2001. Simulating the effects of fluid viscosity on the behaviour of sperm flagella. *Math. Methods Appl. Sci.* 24:1351–1365.

29. Dillon, R. H., L. J. Fauci, and C. Omoto. 2003. Mathematical modeling of axoneme mechanics and fluid dynamics in ciliary and sperm motility. *Dyn. Contin. Discret. I.: Series A Mathematical Analysis.* 10:745–757.

30. Lindemann, C. B. 2007. The geometric clutch as a working hypothesis for future research on cilia and flagella. *Ann. N. Y. Acad. Sci.* 1101: 477–493.

31. Mitran, S. M. 2007. Metachronal wave formation in a model of pulmonary cilia. *Comput. Struct.* 85:763–774.

32. Rikmenspoel, R. 1976. Contractile events in the cilia of Paramecium, Opalina, Mytilus, and Phragmatopoma. *Biophys. J.* 16:445–470.

33. Okuno, M., and Y. Hiramoto. 1979. Direct measurements of the stiffness of echinoderm sperm flagella. *J. Exp. Biol.* 79:235–243.

34. Tuszyński, J. A., T. Luchko, …, J. M. Dixon. 2005. Anisotropic elastic properties of microtubules. *Eur Phys J E Soft Matter*. 17:29–35.

35. Nédélec, F. 2002. Computer simulations reveal motor properties generating stable antiparallel microtubule interactions. *J. Cell Biol.* 158:1005–1015.

36. Gittes, F., B. Mickey, …, J. Howard. 1993. Flexural rigidity of microtubules and actin filaments measured from thermal fluctuations in shape. *J. Cell Biol.* 120:923–934.

37. Elbaum, M., D. Kuchnir Fygenson, and A. Libchaber. 1996. Buckling microtubules in vesicles. *Phys. Rev. Lett.* 76:4078–4081.

38. Cassimeris, L., D. Gard, …, H. P. Erickson. 2001. XMAP215 is a long thin molecule that does not increase microtubule stiffness. *J. Cell Sci.* 114:3025–3033.

39. Camalet, S., and F. Julicher. 2000. Generic aspects of axonemal beating. *New J. Phys.* 2:1–23.

40. Nicastro, D., C. Schwartz, …, J. R. McIntosh. 2006. The molecular architecture of axonemes revealed by cryoelectron tomography. *Science*. 313:944–948.

41. Hastie, A. T., S. P. Marchese-Ragona, …, J. S. Wall. 1988. Structure and mass of mammalian respiratory ciliary outer arm 19S dynein. *Cell Motil. Cytoskeleton.* 11:157–166.

42. Shingyoji, C., H. Higuchi, …, T. Yanagida. 1998. Dynein arms are oscillating force generators. *Nature*. 393:711–714.

43. Satir, P., and T. Matsuoka. 1989. Splitting the ciliary axoneme: implications for a "switch-point" model of dynein arm activity in ciliary motion. *Cell Motil. Cytoskeleton.* 14:345–358.

44. Brokaw, C. J. 1975. Molecular mechanism for oscillation in flagella and muscle. *Proc. Natl. Acad. Sci. USA*. 72:3102–3106.

45. Brokaw, C. J. 2002. Computer simulation of flagellar movement VIII: coordination of dynein by local curvature control can generate helical bending waves. *Cell Motil. Cytoskeleton.* 53:103–124.

46. Hines, M., and J. J. Blum. 1979. Bend propagation in flagella. II. Incorporation of dynein cross-bridge kinetics into the equations of motion. *Biophys. J.* 25:421–441.

47. Machin, K. E. 1958. Wave propagation along flagella. *J. Exp. Biol.* 35:796–806.

48. Camalet, S., F. Julicher, and J. Prost. 1999. Self-organized beating and swimming of internally driven filaments. *Phys. Rev. Lett.* 82: 1590–1593.

49. Julicher, F., and J. Prost. 1997. Spontaneous oscillations of collective molecular motors. *Phys. Rev. Lett.* 78:4510–4513.

50. Lindemann, C. B. 1994. A model of flagellar and ciliary functioning which uses the forces transverse to the axoneme as the regulator of dynein activation. *Cell Motil. Cytoskeleton.* 29:141–154.

51. Lindemann, C. B. 1994. A geometric clutch hypothesis to explain oscillations of the axoneme of cilia and flagella. *J. Theor. Biol.* 168:175–189.

52. Kojima, H., M. Kikumoto, …, K. Oiwa. 2002. Mechanical properties of a single-headed processive motor, inner-arm dynein subspecies-c of *Chlamydomonas* studied at the single molecule level. *J. Biol. Phys.* 28:335–345.

53. Kotani, N., H. Sakakibara, …, K. Oiwa. 2007. Mechanical properties of inner-arm dynein-f (dynein I1) studied with in vitro motility assays. *Biophys. J.* 93:886–894.

54. Riedel-Kruse, I. H., A. Hilfinger, …, F. Jülicher. 2007. How molecular motors shape the flagellar beat. *HFSP J.* 1:192–208.

55. Vernon, G. G., and D. M. Woolley. 2002. Microtubule displacements at the tips of living flagella. *Cell Motil. Cytoskeleton.* 52:151–160.

56. Vernon, G. G., and D. M. Woolley. 2004. Basal sliding and the mechanics of oscillation in a mammalian sperm flagellum. *Biophys. J.* 87:3934–3944.

57. Brokaw, C. J. 2005. Computer simulation of flagellar movement IX. Oscillation and symmetry breaking in a model for short flagella and nodal cilia. *Cell Motil. Cytoskeleton.* 60:35–47.

58. Baconnais, S., R. Tirouvanziam, …, E. Puchelle. 1999. Ion composition and rheology of airway liquid from cystic fibrosis fetal tracheal xenografts. *Am. J. Respir. Cell Mol. Biol.* 20:605–611.

59. Matsui, H., V. E. Wagner, …, R. C. Boucher. 2006. A physical linkage between cystic fibrosis airway surface dehydration and *Pseudomonas aeruginosa* biofilms. *Proc. Natl. Acad. Sci. USA*. 103:18131–18136.

60. Yeates, D. B., G. J. Besseris, and I. Wong. 1997. Physiochemical properties of mucus and its propulsion. *In* The Lung: Scientific Foundation. R. G. Crystal, J. B. West, and E. R. Weibel, …, editors. Raven Publishers, Philadelphia, PA. 487–503.

61. Braga, P. C., L. Allegra, …, A. Mocchi. 1992. A new rheometer with special features designed for bronchial mucus analysis in clinical practice. *Biorheology.* 29:285–293.

62. Puchelle, E., J. M. Zahm, and F. Aug. 1981. Viscoelasticity, protein content and ciliary transport rate of sputum in patients with recurrent and chronic bronchitis. *Biorheology.* 18:659–666.

63. Machemer, H. 1972. Ciliary activity and the origin of metachrony in Paramecium: effects of increased viscosity. *J. Exp. Biol.* 57:239–259.

64. Gheber, L., A. Korngreen, and Z. Priel. 1998. Effect of viscosity on metachrony in mucus propelling cilia. *Cell Motil. Cytoskeleton.* 39:9–20.

65. Andrade, Y. N., J. Fernandes, …, M. A. Valverde. 2005. TRPV4 channel is involved in the coupling of fluid viscosity changes to epithelial ciliary activity. *J. Cell Biol.* 168:869–874.

66. Johnson, N. T., M. Villalón, …, P. Verdugo. 1991. Autoregulation of beat frequency in respiratory ciliated cells. Demonstration by viscous loading. *Am. Rev. Respir. Dis.* 144:1091–1094.

67. Ohmuro, J., and S. Ishijima. 2006. Hyperactivation is the mode conversion from constant-curvature beating to constant-frequency beating under a constant rate of microtubule sliding. *Mol. Reprod. Dev.* 73:1412–1421.

68. Sanderson, M. J., and E. R. Dirksen. 1986. Mechanosensitivity of cultured ciliated cells from the mammalian respiratory-tract: implications for the regulation of mucociliary transport. *Proc. Natl. Acad. Sci. USA.* 83:7302–7306.

69. Dirksen, E. R. 1982. Ciliary basal body morphogenesis: the early events. *Symp. Soc. Exp. Biol.* 35:439–463.

70. Resnick, A., and U. Hopfer. 2007. Force-response considerations in ciliary mechanosensation. *Biophys. J.* 93:1380–1390.

71. Winters, S. L., C. W. Davis, and R. C. Boucher. 2007. Mechanosensitivity of mouse tracheal ciliary beat frequency: roles for Ca^{2+}, purinergic signaling, tonicity, and viscosity. *Am. J. Physiol. Lung Cell. Mol. Physiol.* 292:L614–L624.